

Detecting causality in multivariate time series via non-uniform embedding

Ziyu Jia¹, Youfang Lin¹, Yunxiao Liu¹, Zehui Jiao¹, Yan Ma², Jing Wang^{*,1}

¹ School of Computer and Information Technology, Beijing Jiaotong University, Beijing 100044, PR China

*² Division of Interdisciplinary Medicine and Biotechnology, Department of Medicine,
Beth Israel Deaconess Medical Center/ Harvard Medical School, Boston, MA, USA*

Abstract

Causal analysis based on non-uniform embedding schemes is an important way to detect the underlying interactions between dynamic systems. However, there are still some obstacles to estimate high-dimensional conditional mutual information and form optimal mixed embedding vector in traditional non-uniform embedding schemes. In this study, we present a new non-uniform embedding method framed in information theory to detect causality for multivariate time series, named LM-PMIME, which integrates the low-dimensional approximation of conditional mutual information and the mixed search strategy for the construction of the mixed embedding vector. We apply the proposed method to simulations of linear stochastic, nonlinear stochastic, and chaotic systems, demonstrating its superiority over partial conditional mutual information from mixed embedding (PMIME) method. Moreover, the proposed method works well for multivariate time series with weak coupling strengths, especially for chaotic systems. In the actual application, we show its applicability to epilepsy multi-channel electrocorticographic recordings.

Keywords: causal analysis; non-uniform embedding; multivariate time series; conditional mutual information.

1. Introduction

In recent years, various time series analysis methods have been proposed to identify interactions between complex systems, especially the study of causality has attracted wide attention of researchers. There are two classic methods in the time series causal analysis: Granger causality [1] and transfer entropy [2, 3]. Both methods are based on time series prediction for causal analysis. In addition, the relationship between Granger causality and transfer entropy is demonstrated [4]: the two methods are equivalent under Gaussian assumptions. Furthermore, Schindlerova et al. [5] extend the equivalence of the two causality methods under the condition of non-Gaussian probability density distributions.

With the development of multivariate state space reconstruction, different embedding schemes [6–8] are used in Granger causality and transfer entropy. The common idea of those embedding schemes is to reconstruct the past of the whole system represented by all variables with reference to the target variable, in order to form a mixed embedding vector containing the most significant past variables to explain the target variable. Non-uniform embedding schemes are proposed to overcome the problems of arbitrariness and redundancy in uniform embedding schemes [8]. Vlachos et al. propose a causality measure based on the mixed embedding scheme for bivariate time series: the conditional mutual information from mixed embedding (MIME) [9]. Kugiumtzis et al. extend the measure MIME to multivariate time series and form the partial MIME (PMIME) [10]. The PMIME addresses successfully the problem of detecting direct causal effects in the multivariate variables. In addition, it is gradually applied to complex systems such as physiology [11, 12] and finance [13, 14].

Although the causal analysis based on non-uniform embedding schemes has practical advantages, there are still some key shortcomings that need to be overcome. One shortcoming is the curse of dimensionality, which makes the estimation of mutual information inaccurate as the dimension of the embedded space increases [15–18]. Another shortcoming is related to the mixed embedding vector. The greedy strategy

uses a sequential forward approach to select the lagged variables and finally form the mixed embedding vector [8–10]. That is to say, the lagged variables that have been embedded will not be changed in the mixed embedding vector. As the iteration increases, more lagged variables are selected until the final mixed embedding vector is formed. Therefore, the inaccuracy of the initial embedding will have a large impact on the results. For example, there are three variables A, B, and C where the target variable is A. Suppose driving variable C has an effect on variable A and variable B, making A and B highly correlated. Then one of the lagged variables B may be embedded in the first iteration using the greedy strategy. However, the true driving variable C will be ignored resulting in an initial embedding error. The above shortcomings will be highlighted when there are multivariate time series of weak causal coupling strengths in practical applications.

We recently put forward a new non-uniform embedding method named LM-PMIME for multivariate time series according to the low-dimensional approximation of conditional mutual information and the mixed search strategy. The main idea of the proposed method is to reduce the dimension of the embedded space by replacing the original estimate with a low-dimensional approximation of conditional mutual information. In addition, a mixed strategy instead of the greedy strategy was used as an embedded strategy to optimize initial embedding. The proposed method works well for multivariate time series with weak coupling strengths.

The rest of the paper is organized as follows. In Section 2, we present the whole structure of multivariate non-uniform embedding in accordance with the low dimensional approximation of CMI and a mixed search strategy. In Section 3, we perform a large number of simulation experiments in order to verify the effectiveness of the proposed method. In Section 4, by analyzing the electrocorticographic (ECoG) recordings from an epileptic patient, the applicability of the proposed method to actual data is shown. Finally, a summary is presented in Section 5.

2. Method

In this section, we first introduce the traditional PMIME method. Then we expound a low dimensional approximation of conditional mutual information and a mixed search strategy. Finally, we present the LM-PMIME method for multivariable non-uniform embedding.

2.1. PMIME Method

Partial conditional mutual information from mixed embedding (PMIME), a generalization of conditional mutual information from mixed embedding (MIME) for bivariate time series [9], is developed by Kugiumtzis et al. [10] for estimating the directional coupling in multivariate time series. Let K variables $X, Y, Z_1, \dots, Z_{K-2}$ constitute an overall dynamical system $\{x_t, y_t, z_{1,t}, \dots, z_{K-2,t}\}_{t=1}^n$. Suppose that the driving subsystem is X and the target subsystem is Y . In other words, the current value of variable Y is affected by the past of variable X . $Z = \{Z_1, \dots, Z_{K-2}\}$ represent the remaining subsystems.

We estimate the causal effect of X on Y conditioned by $Z = \{Z_1, \dots, Z_{K-2}\}$. It is necessary to form a set of variables representing the past of the subsystems. The lags of X , Y and Z are sought within a range given by a maximum lag for each variable, e.g., L_x for X and L_y for Y . W_t is defined as the set of all lagged variables at time t , containing the parts $x_t, x_{t-1}, \dots, x_{t-L_x}$ of X and the same for Y and Z . It is usually assumed that the maximum lag L for all variables is the same ($L_x = L_y = L_z$). The larger the value of L , the more lagged variables are included in W_t . The key step of the PMIME method is to form the mixed embedding vector $\mathbf{v}_t \in W_t$ using non-uniform embedding. Greedy forward selection and a stopping criterion are applied to the process of embedding. The detailed method is described below as follows :

1. Initialize an empty embedding vector $\mathbf{v}_t^0 = \emptyset$.

2. At the first iteration $k = 1$, we search the embedding vector $w_t^1 \in W_t$ being most correlated to \mathbf{y}_t :

$$w_t^1 = \arg \max_{w \in W_t} I(\mathbf{y}_t; w) \quad (1)$$

where $I(\cdot)$ represents mutual information. Mutual information is estimated by the k-nearest neighbors (k-NNs) estimator. Then we have $\mathbf{v}_t^1 = [w_t^1]$. At the same time, w_t^1 was removed from W_t .

3. At the iteration $k > 1$, the mixed embedding vector is augmented by the component w_t^k of W_t , giving most information about \mathbf{y}_t additionally to the information already contained in $\mathbf{v}_t^{k-1} = [w_t^1, \dots, w_t^{k-1}]$. w_t^k will be tested by a standard through computing the maximum conditional mutual information (CMI), $w_t^k = \arg \max_{w \in W_t} I(\mathbf{y}_t; w | \mathbf{v}_t^{k-1})$, i.e., at the iteration $k = 2$, $w_t^2 = \arg \max_{w \in W_t} I(\mathbf{y}_t; w | \mathbf{v}_t^1)$, where the conditional mutual information is estimated by the k-NNs estimator, and the mixed embedding vector is $\mathbf{v}_t^2 = [w_t^1, w_t^2]$. Using greedy forward method each w_t^k will be embedded in the already embedded vector \mathbf{v}_t^{k-1} until the process stops. The termination criterion is quantified as :

$$I(\mathbf{y}_t; \mathbf{v}_t^{k-1}) / I(\mathbf{y}_t; \mathbf{v}_t^k) > A \quad (2)$$

where the threshold $A < 1$ and the general value of A is 0.95 or 0.97 in [9,10]. That is, the additional information of w_t^k selected at the iteration k is not large enough. The embedding process will stop and we have the mixed embedding vector $\mathbf{v}_t = \mathbf{v}_t^{k-1}$. And any combination of the lagged variables $X, Y, Z_1, \dots, Z_{K-2}$ may be included in \mathbf{v}_t .

4. To quantify the causal effect of X on Y conditioned by the other variables in Z , the index is defined as

$$R_{X \rightarrow Y|Z} = \frac{I(\mathbf{y}_t; \mathbf{v}_t^x | \mathbf{v}_t^y, \mathbf{v}_t^z)}{I(\mathbf{y}_t; \mathbf{v}_t)} \quad (3)$$

where \mathbf{v}_t^x represents the component of X in \mathbf{v}_t . And the same for \mathbf{v}_t^y and \mathbf{v}_t^z . The causal effect of X to Y depends on the components of X in \mathbf{v}_t^x .

2.2. The Proposed Method

2.2.1. Low Dimensional Approximation of CMI

With the increase of the mixed embedding vector dimension, the estimation of CMI becomes less reliable. The curse of dimensionality appears as the dimension increases. Because an increasing volume of state space makes the estimation of entropy rates progressively decrease towards zero [19]. Therefore, in order to overcome the problems caused by computing high-dimensional CMI, the low-dimensional approximation of CMI is a better alternative. The low-dimensional approximation can reduce the computational cost and improve the accuracy of conditional mutual information estimation.

The low-dimensional approximation of CMI is studied by researchers in the field of information theory based on feature selection [20–25]. Brown et al. [17] emphasize that lots of feature selection heuristics are all approximate iterative maximisers of the conditional likelihood, which can be interpreted in a unifying framework of conditional likelihood maximisation under certain assumptions of independence. Consequently, the methods are summarized as a parameterized general standard:

$$I(w; \mathbf{y}_t) - \beta \sum_{w_i \in \mathbf{v}_t} I(w; w_i) + \gamma \sum_{w_i \in \mathbf{v}_t} I(w; w_i | \mathbf{y}_t) \quad (4)$$

where the difference between different standards depends on the parameters (β and γ), for example, the JMI standard [21] can be obtained with $\beta = \gamma = 1/|\mathbf{v}_t|$. β and γ are different in standards such as MRMR standard [23], and CIFE standard [24]. Recent studies have shown that higher-order feature

interactions are considered to optimize feature selection standard [18]. Therefore, we need to consider the second-order interactions between the features compared to Eq (4), such as $I(w; w_j|w_i)$.

$$I(w; \mathbf{y}_t) - \beta \sum_{w_i \in \mathbf{v}_t} I(w; w_i) + \gamma \sum_{w_i \in \mathbf{v}_t} I(w; w_i | \mathbf{y}_t) - \delta \sum_{w_i \in \mathbf{v}_t} \sum_{w_j \in \mathbf{v}_t; i \neq j} I(w; w_j | w_i) \quad (5)$$

where $\beta = \gamma = 1/|\mathbf{v}_t|$ and $\delta = 1/|\mathbf{v}_t|(|\mathbf{v}_t| - 1)$.

2.2.2. Mixed Search Strategy

A correct search strategy is important for building the mixed embedding vector. Because the greedy search strategy has high computational efficiency and good practicability, it has become the preferred strategy for embedding. However, the greedy strategy uses a sequential forward approach to select lagged variables, which rely heavily on the initial embedded vector. That is to say, the initial embedded vector is not accurate and the subsequent selection will get worse.

In order to solve the above problem, we propose a mixed strategy to avoid inaccuracies in the initial embedding. The mixed strategy consists of two strategies: the traversal strategy and the greedy strategy. The application of the strategy is determined by defining a strategy adjustment factor m . Assuming that a number of iterations is k , the traversal strategy is applied when $1 < k \leq m$. And the greedy strategy is applied when $k > m$.

2.2.3. LM-PMIME Method

We put forward the LM-PMIME method for estimating the directional coupling in multivariate time series according to the low-dimensional approximation of conditional mutual information and the mixed search strategy. In the LM-PMIME method, the mixed strategy determines the way to select lagged variables. But whether the variable will be embedded depends on the low dimensional approximation of conditional mutual information. Fig.1 is an illustration of the flow of the LM-PMIME method.

The detailed LM-PMIME method is as follows:

1. Initialize an empty embedding vector $\mathbf{v}_t^0 = \emptyset$.
2. At the first iteration $k = 1$, we search the embedding vector $w_t^1 \in W_t$ being most correlated to \mathbf{y}_t :

$$w_t^1 = \arg \max_{w \in W_t} I(\mathbf{y}_t; w) \quad (6)$$

Then we have $\mathbf{v}_t^1 = [w_t^1]$.

3. At the iteration $1 < k \leq m$, w_t^k will be tested by a standard through computing the maximum value of the low dimensional approximation of CMI.

$$w_t^k = \arg \max_{w \in W_t} I(w; \mathbf{y}_t) - \beta \sum_{w_i \in \mathbf{v}_t^{k-1}} I(w; w_i) + \gamma \sum_{w_i \in \mathbf{v}_t^{k-1}} I(w; w_i | \mathbf{y}_t) - \delta \sum_{w_i \in \mathbf{v}_t^{k-1}} \sum_{w_j \in \mathbf{v}_t^{k-1}; i \neq j} I(w; w_j | w_i) \quad (7)$$

The traversal strategy is applied to select w_t^k , i.e., at the iteration $k = 2$ and $m = 3$, w_t^2 needs to be selected. First clear the already embedded vector \mathbf{v}_t^1 and select $k - 1$ lagged variables as $\mathbf{v}_t^1 \in W_t$. The remaining lagged variables in W_t are computed as candidate lagged variables for w_t^2 . After the first calculation is finished, continue to select $k - 1$ lagged variables different from the previous one as \mathbf{v}_t^1 to compute CMI. Until the combination of lagged variables acting as \mathbf{v}_t^1 traverses W_t , the \mathbf{v}_t^2 can be determined by the embedding standard. Then $k = k + 1$.

4. At the iteration $k > m$, greedy strategy is used. Each w_t^k will be embedded in the already embedded vector \mathbf{v}_t^{k-1} until the process stops. The standard of low dimensional approximation is still used before stopping.

5. The termination criterion is quantified as

$$I(\mathbf{y}_t; \mathbf{v}_t^{k-1})/I(\mathbf{y}_t; \mathbf{v}_t^k) > A \quad (8)$$

where the threshold $A < 1$ and the general value of A is 0.95 or 0.97 in [9, 10]. Finally, we have the mixed embedding vector $\mathbf{v}_t = \mathbf{v}_t^{k-1}$.

6. To quantify the causal effect of X on Y , the index is defined as :

$$R_{X \rightarrow Y|Z} = \frac{I(\mathbf{y}_t; \mathbf{v}_t^x | \mathbf{v}_t^y, \mathbf{v}_t^z)}{I(\mathbf{y}_t; \mathbf{v}_t)} \quad (9)$$

where \mathbf{v}_t^x represents the component of X in \mathbf{v}_t . And the same for \mathbf{v}_t^y and \mathbf{v}_t^z .

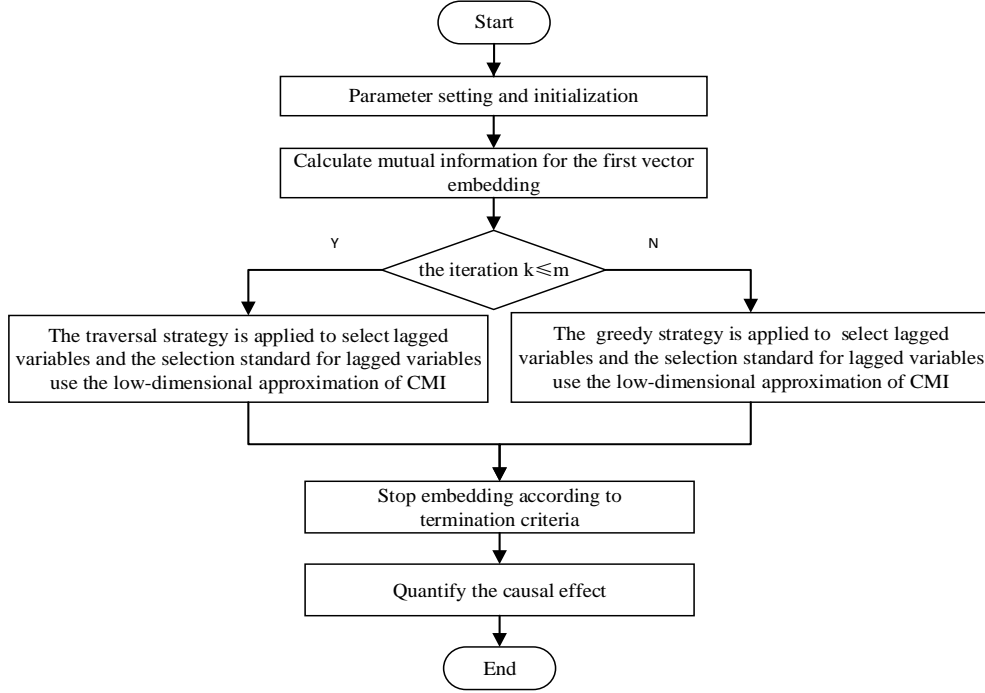


Figure 1 The Flow chart of the LM-PMIME method.

3. Simulation study

In this section, we perform a series of causal analysis simulation experiments using linear stochastic, nonlinear stochastic, and chaotic systems. The experiments compare the differences between the proposed LM-PMIME method and the traditional PMIME method for time series with different lengths or coupling strengths. The experiments also add a comparison method M-PMIME, which improve the search strategy without using low-dimensional approximation.

We calculate all methods on 100 realizations from each system to assess statistically the sensitivity and specificity of the methods. The connections between variables are classified as coupled directions and uncoupled directions to compute the confusion matrix: TP (ture positive), FP (false positive), TN (true negative), and FN (false negative), where sensitivity = $TP/(TP + FN)$, specificity = $TN/(TN + FP)$, and F1 score = $2TP/(2TP + FP + FN)$.

The accuracy of the estimated mutual information is vital for embedding vector selection [23]. The two most common methods for estimating mutual information are the histogram and kernel methods.

The former one is time efficient but not highly accurate [26]. The latter one has high accuracy but comes with huge computational pressure [27]. We applied the k-nearest neighbors (k-NNs) method to estimate mutual information, because the k-NNs estimator is suitable for high-dimensional data [28].

In the following results, the performance of LM-PMIME and a comparison to M-PMIME and PMIME are presented for multivariate time series with different lengths or coupling strengths.

3.1. Linear multivariate stochastic process

The first system is a linear vector autoregressive (VAR) process which is composed of order 4 in 5 time series (model 1 in [29]).

$$\begin{cases} x_{1,t} = 0.4x_{1,t-1} - 0.5x_{1,t-2} + 0.4x_{5,t-1} + e_{1,t} \\ x_{2,t} = 0.4x_{2,t-1} - 0.3x_{1,t-4} + 0.4x_{5,t-2} + e_{2,t} \\ x_{3,t} = 0.5x_{3,t-1} - 0.7x_{3,t-2} - 0.3x_{5,t-3} + e_{3,t} \\ x_{4,t} = 0.8x_{4,t-3} + 0.4x_{1,t-2} + 0.3x_{2,t-2} + e_{4,t} \\ x_{5,t} = 0.7x_{5,t-1} - 0.5x_{5,t-2} - 0.4x_{4,t-1} + e_{5,t} \end{cases} \quad (10)$$

where $e_{i,t}$, $i = 1, \dots, 5$, are Gaussian noise with zero mean and unit covariance matrix. $X_1 \rightarrow X_2$, $X_1 \rightarrow X_4$, $X_2 \rightarrow X_4$, $X_4 \rightarrow X_5$, $X_5 \rightarrow X_1$, $X_5 \rightarrow X_2$, and $X_5 \rightarrow X_3$ are the true causal connections in this process.

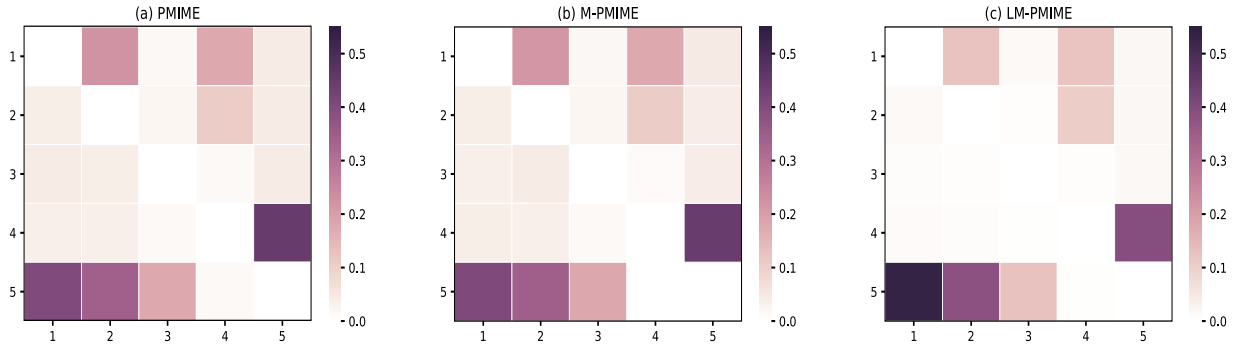


Figure 2 Matrix representation of causality for the linear VAR process. Retrieved by traditional PMIME method (a), M-PMIME method (b), and LM-PMIME method (c) with k-NNs estimator. The length of the time series is 512. $m = 2$ is used for the M-PMIME method and the LM-PMIME method. The remaining parameters of the three methods are the same ($L = 6, A = 0.97$). Color maps for the mean values of coupling measurements are obtained from 100 realizations of the linear VAR process. The direction of causal influence is from row to column in the matrix. The true causal connections in this linear VAR process are at the matrix elements (1, 2), (1, 4), (2, 4), (4, 5), (5, 1), (5, 2) and (5, 3).

We use $A = 0.97$ and $L = 6$, which matches the larger lag for the three methods in the process. In addition, the LM-PMIME method and the M-PMIME method use the parameter $m = 2$. The results from linear VAR process with the time series length of 512 are shown in Fig 2. The direction of causal influence is from row to column in the matrix representation, e. g. the causal connection $X_1 \rightarrow X_2$ is represented as (1, 2) in the matrix representation. Hence, true causal connections in this process are at the matrix elements (1, 2), (1, 4), (2, 4), (4, 5), (5, 1), (5, 2) and (5, 3). The mean values of coupling measured by the three methods are positive and high on these matrix elements. It is proved that the three methods have good sensitivity to true couplings. However, Fig 2 shows that there are lots of false positives in the traditional method using high-dimensional CMI. In contrast, the LM-PMIME method

has better performance than the other two methods, because the method reduces false positives. The sensitivity, specificity, and F1 score are obtained from 100 realizations of linear VAR process with varying length of time series. The values of the specific indexes are listed in Table I. The F1 score of LM-PMIME method has better results on linear VAR process with different time series lengths. Furthermore, the F1 score calculated by the LM-PMIME method increases as the length of the time series increases. These better results are likely due to the great improvement of specificity by the proposed method. At the same time, the F1 score reflects that PMIME method and M-PMIME method have achieved similar results in the linear VAR process. It shows that the mixed strategy does not work in this process. However, the following experiments show that the mixed strategy works well on the chaotic system.

TABLE I Sensitivity, specificity, and F1 score are obtained from 100 realizations of linear VAR process with varying length of time series for the three different methods. $A = 0.97$ and $L = 6$ are the parameters common to the three methods. In addition, the LM-PMIME method and the M-PMIME method use the parameter $m = 2$.

	Sensitivity	Specificity	F1 score
$n = 256$			
PMIME	0.988	0.492	0.600
M-PMIME	0.989	0.481	0.596
LM-PMIME	0.797	0.741	0.647
$n = 512$			
PMIME	1.000	0.567	0.643
M-PMIME	0.994	0.727	0.645
LM-PMIME	0.855	0.763	0.693
$n = 1024$			
PMIME	1.000	0.697	0.719
M-PMIME	0.940	0.729	0.713
LM-PMIME	0.877	0.807	0.739

3.2. Nonlinear multivariate stochastic process 1

The first nonlinear VAR process is of order 5 in four variables $\text{NLVAR}_4(5)$ with Gaussian noise (model 1 in [30]). The true causal connections in the process are $X_1 \rightarrow X_3$, $X_2 \rightarrow X_1$, $X_2 \rightarrow X_3$, and $X_4 \rightarrow X_2$.

$$\begin{cases} x_{1,t} = 0.8x_{1,t-1} + 0.65x_{2,t-4} + e_{1,t} \\ x_{2,t} = 0.6x_{2,t-1} + 0.6x_{4,t-5}^2 + e_{2,t} \\ x_{3,t} = 0.5x_{3,t-3} - 0.6x_{1,t-1}^2 + 0.4x_{2,t-4} + e_{3,t} \\ x_{4,t} = 1.2x_{4,t-1} - 0.7x_{4,t-2} + e_{4,t} \end{cases} \quad (11)$$

For all methods, the results from 100 realizations of the $\text{NLVAR}_4(5)$ with the time series length of 512 are shown in Fig 2. $m = 2$ is used for the M-PMIME method and the LM-PMIME method. The remaining parameters of the three methods are the same ($L = 8$, $A = 0.97$). The true causal connections are expressed as matrix elements (1, 3), (2, 1), (2, 3), and (4, 2). The traditional PMIME method fails to detect the true causal connection $X_2 \rightarrow X_3$ for any time series length. However, both LM-PMIME method and M-PMIME method successfully detect all correct causal connections. Furthermore, the coupling measured by the latter method is higher than the former method. The sensitivity, specificity, and F1 score are obtained from the $\text{NLVAR}_4(5)$ process with varying length of time series. The values of sensitivity, specificity, and F1 score are listed in Table II. Both LM-PMIME method and M-PMIME method achieve good results according to F1 score. The latter method still has a high F1 score. It shows that the proposed mixed strategy has a good effect in the $\text{NLVAR}_4(5)$.

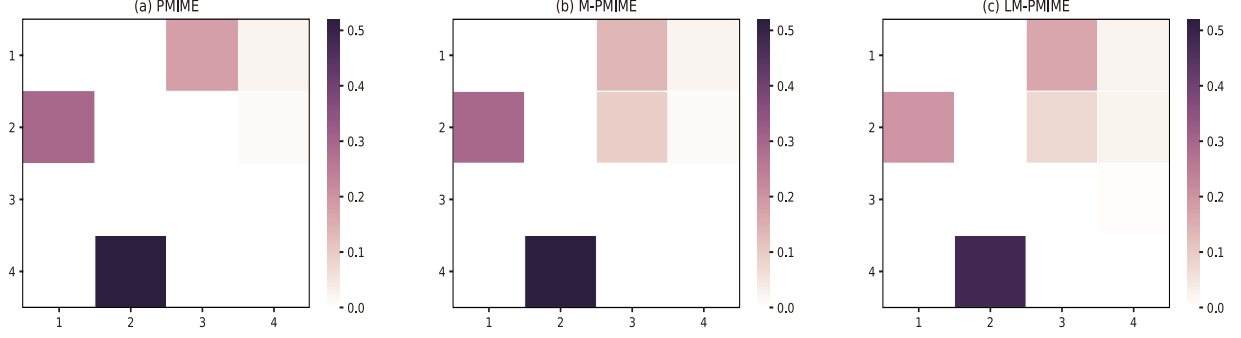


Figure 3 Matrix representation of causality for NLVAR₄(5). Retrieved by traditional PMIME method (a), M-PMIME method (b), and LM-PMIME method (c) with k-NNs estimator. The length of the time series is 512. $m = 2$ is used for the M-PMIME method and the LM-PMIME method. The remaining parameters of the three methods are the same ($L = 8, A = 0.97$). Color maps for the mean values of coupling measurements are obtained from 100 realizations of NLVAR₄(5). The direction of causal influence is from row to column in the matrix. The true causal connections in NLVAR₄(5) are at the matrix elements (1,3), (2,1), (2,3), (4,2).

TABLE II Sensitivity, specificity, and F1 score are obtained from 100 realizations of NLVAR₄(5) with varying length of time series for the three different methods. $A = 0.97$ and $L = 8$ are the parameters common to the three methods. In addition, the LM-PMIME method and the M-PMIME method use the parameter $m = 2$

	Sensitivity	Specificity	F1 score
$n = 256$			
PMIME	0.750	0.825	0.659
M-PMIME	0.862	0.822	0.719
LM-PMIME	0.860	0.774	0.678
$n = 512$			
PMIME	0.750	0.890	0.721
M-PMIME	0.867	0.890	0.789
LM-PMIME	0.873	0.830	0.733
$n = 1024$			
PMIME	0.905	0.861	0.780
M-PMIME	0.875	0.953	0.868
LM-PMIME	0.750	0.954	0.794

3.3. Nonlinear multivariate stochastic process 2

The second nonlinear VAR process is of order 1 in three variables NLVAR₃(1) (model 7 in [31]).

$$\begin{cases} x_{1,t} = 3.4x_{1,t-1}(1 - x_{1,t-1}^2)e^{-x_{1,t-1}^2} + 0.4e_{1,t} \\ x_{2,t} = 3.4x_{2,t-1}(1 - x_{2,t-1}^2)e^{-x_{2,t-1}^2} + 0.5x_{1,t-1}x_{2,t-1} + 0.4e_{2,t} \\ x_{3,t} = 3.4x_{3,t-1}(1 - x_{3,t-1}^2)e^{-x_{3,t-1}^2} + 0.3x_{2,t-1} + 0.5x_{1,t-1}^2 + 0.4e_{3,t} \end{cases} \quad (12)$$

The true causal connections in NLVAR₃(1) are $X_1 \rightarrow X_2$, $X_1 \rightarrow X_3$, $X_2 \rightarrow X_3$. The results obtained from 100 realizations of the nonlinear VAR process are shown in Fig 4 for $n = 512$, $A = 0.97$, $L = 6$. The strategy adjustment factor $m = 3$ determines the application of the strategies for LM-PMIME method and M-PMIME method. The true causal connections in NLVAR₃(1) are represented at the matrix elements (1,2), (1,3), and (2,3). For the three methods, the mean values of coupling measurements on these matrix elements are positive and high. It turns out that all methods have good sensitivity to true couplings. But there are many false positives in the traditional methods using high-dimensional CMI. Hence, the LM-PMIME method significantly outperforms the others. The sensitivity, specificity, and F1 score are obtained from NLVAR₃(1) by gradually increasing the time series length from 256 to 1024. The values

of the specific indexes are listed in Table III. The F1 score of LM-PMIME method has better results on $NLVAR_3(1)$ with different time series lengths. In addition, the F1 score will increase as the length of the time series increases. The low-dimensional approximation of CMI can greatly improve specificity, although mixed strategy does not work in $NLVAR_3(1)$.

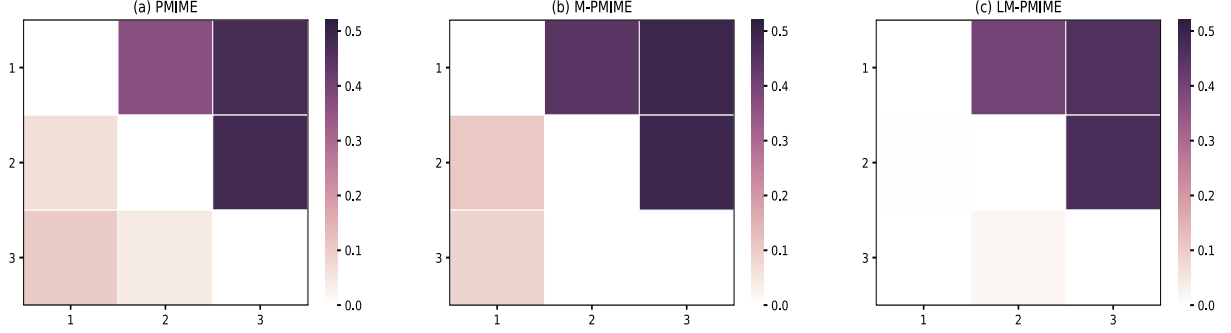


Figure 4 Matrix representation of causality for $NLVAR_3(1)$. Retrieved by traditional PMIME method (a), M-PMIME method (b), and LM-PMIME method (c) with k-NNs estimator. The length of the time series is 512. $m = 3$ is used for the M-PMIME method and the LM-PMIME method. The remaining parameters of the three methods are the same ($L = 6$, $A = 0.97$). Color maps for the mean values of coupling measurements are obtained from 100 realizations of $NLVAR_3(1)$. The direction of causal influence is from row to column in the matrix. The true causal connections in $NLVAR_3(1)$ are at the matrix elements (1,2), (1,3), (2,3).

TABLE III Sensitivity, specificity, and F1 score are obtained from 100 realizations of $NLVAR_3(1)$ with varying length of time series for the three different methods. $A = 0.97$ and $L = 6$ are the parameters common to the three methods. In addition, the LM-PMIME method and the M-PMIME method use the parameter $m = 3$.

	Sensitivity	Specificity	F1 score
$n = 256$			
PMIME	0.973	0.650	0.737
M-PMIME	0.976	0.615	0.712
LM-PMIME	0.860	0.844	0.792
$n = 512$			
PMIME	1.000	0.681	0.758
M-PMIME	1.000	0.662	0.748
LM-PMIME	0.950	0.887	0.873
$n = 1024$			
PMIME	1.000	0.860	0.877
M-PMIME	1.000	0.790	0.827
LM-PMIME	0.989	0.892	0.896

3.4. Coupled Henon maps

The system of K coupled chaotic Henon maps defined as

$$\begin{cases} x_{1,t} = 1.4 - x_{1,t-1}^2 + 0.3x_{1,t-2} \\ x_{i,t} = 1.4 - (Cx_{i-1,t-1} + (1-C)x_{i,t-1})^2 + 0.3x_{i,t-2} \end{cases} \quad \text{for } i = 2, \dots, K \quad (13)$$

$X_{i-1} \rightarrow X_i$, where $i = 2, \dots, K$, are the true causal connections in the K coupled chaotic Henon maps. The results from 100 realizations of the coupled Henon maps with the coupling strength $C = 0.1$ are shown in Fig 5 for $n = 1024$, $K = 6$, $A = 0.95$, $L = 5$, $m = 2$. In addition to this, the results of only changing the coupling strength $C = 0.3$ are shown in Fig 6. The true causal connections in the coupled Henon maps are at the matrix elements $(i-1, i)$, where $i = 2, \dots, 6$. There is almost no false positive

for all methods. However, Fig 5 and Fig 6 illustrate that the proposed methods have better performance than the traditional method when there are true causal connections. All methods will detect stronger causal connections as the coupling strength C of the system increases. The sensitivity, specificity, and F1 score are obtained from coupled Henon maps with the variables K from 3 to 9. The values of the specific indexes are listed in Table IV and Table V. The results show that the F1 score of the LM-PMIME method is higher than the others when the coupling strength is low. Although the F1 score may be affected by the number of variables K in the simulation experiments, the F1 score for the LM-PMIME method is above 0.9. The LM-PMIME method and the M-PMIME method greatly improve the specificity, especially the former method. It is proved that both low-dimensional approximation of CMI and the mixed strategies play an important role in coupled Henon maps when the coupling strength is low.

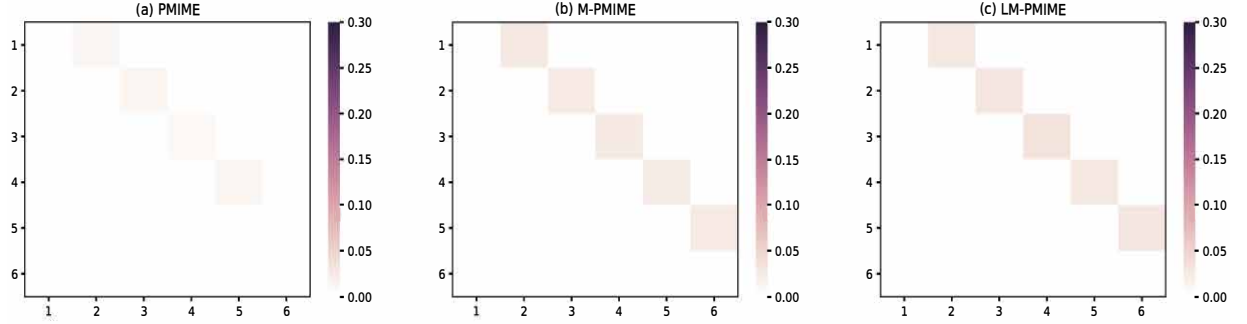


Figure 5 Matrix representation of causality for $K = 6$ variables of the coupled Henon maps ($C = 0.1$). Retrieved by traditional PMIME method (a), M-PMIME method (b), and LM-PMIME method (c) with k-NNs estimator. The length of the time series is 1024. $m = 2$ is used for the M-PMIME method and the LM-PMIME method. The remaining parameters of the three methods are the same ($L = 5$, $A = 0.95$). Color maps for the mean values of coupling measurements are obtained from 100 realizations of the coupled Henon maps. The direction of causal influence is from row to column in the matrix. The true causal connections in the coupled Henon maps are at the matrix elements $(i - 1, i)$, where $i = 2, \dots, 6$.

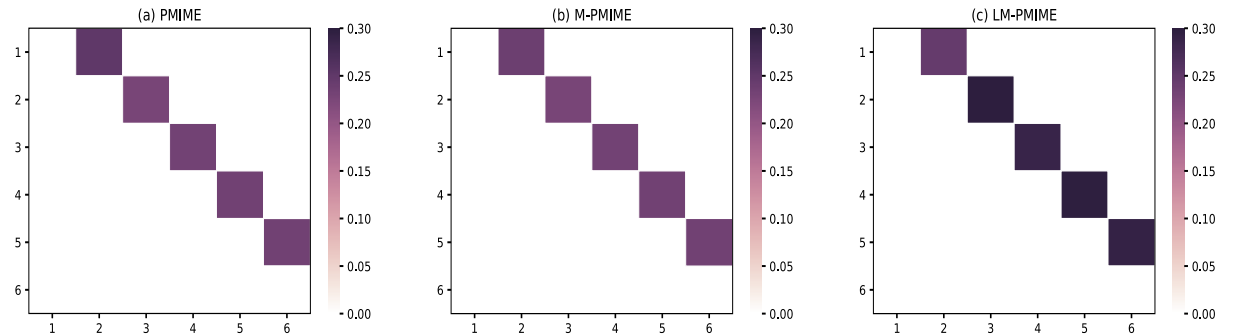


Figure 6 Matrix representation of causality for $K = 6$ variables of the coupled Henon maps ($C = 0.3$). Retrieved by traditional PMIME method (a), M-PMIME method (b), and LM-PMIME method (c) with k-NNs estimator. The length of the time series is 1024. $m = 2$ is used for the M-PMIME method and the LM-PMIME method. The remaining parameters of the three methods are the same ($L = 5$, $A = 0.95$). Color maps for the mean values of coupling measurements are obtained from 100 realizations of the coupled Henon maps. The direction of causal influence is from row to column in the matrix. The true causal connections in the coupled Henon maps are at the

matrix elements $(i-1, i)$, where $i = 2, \dots, 6$.

TABLE IV Sensitivity, specificity, and F1 score are obtained from 100 realizations of K variables of the coupled Henon maps ($C = 0.1$) for the three different methods. $A = 0.95$ and $L = 5$ are the parameters common to the three methods. In addition, the LM-PMIME method and the M-PMIME method use the parameter $m = 2$.

	Sensitivity	Specificity	F1 score
$K = 3$			
PMIME	0.175	1.000	0.297
M-PMIME	0.715	1.000	0.834
LM-PMIME	0.945	1.000	0.972
$K = 6$			
PMIME	0.217	1.000	0.357
M-PMIME	0.674	1.000	0.806
LM-PMIME	0.926	0.998	0.950
$K = 9$			
PMIME	0.204	1.000	0.338
M-PMIME	0.700	1.000	0.824
LM-PMIME	0.895	0.998	0.904

TABLE V Sensitivity, specificity, and F1 score are obtained from 100 realizations of K variables of the coupled Henon maps ($C = 0.3$) for the three different methods. $A = 0.95$ and $L = 5$ are the parameters common to the three methods. In addition, the LM-PMIME method and the M-PMIME method use the parameter $m = 2$.

	Sensitivity	Specificity	F1 score
$K = 3$			
PMIME	1.000	1.000	1.000
M-PMIME	1.000	1.000	1.000
LM-PMIME	1.000	1.000	1.000
$K = 6$			
PMIME	1.000	1.000	1.000
M-PMIME	1.000	1.000	1.000
LM-PMIME	1.000	1.000	1.000
$K = 9$			
PMIME	1.000	1.000	1.000
M-PMIME	1.000	1.000	1.000
LM-PMIME	1.000	1.000	1.000

3.5. Coupled Lorenz system

Next we study a chaotic system of three coupled identical Lorenz oscillators defined as

$$\begin{cases} \dot{x}_1 = -10x_1 + 10y_1, & \dot{x}_i = -10x_i + 10y_i + C(x_{i-1} - x_i), \\ \dot{y}_1 = -x_1z_1 + 28x_1 - y_1, & \dot{y}_i = -x_iz_i + 28x_i - y_i, \\ \dot{z}_1 = x_1y_1 - \frac{8}{3}z_1, & \dot{z}_i = x_iy_i - \frac{8}{3}z_i, \end{cases} \quad (14)$$

where $i = 2, 3$. Solving the differential equations by the explicit Runge-Kutta (4,5) method in MATLAB. In addition, the time series are generated at a sampling time of 0.05 time units. The true causal connections in the three coupled Lorenz oscillators are $X_{i-1} \rightarrow X_i$, where $i = 2, 3$.

The results from 100 realizations of the three coupled Lorenz oscillators with the coupling strength $C = 3$ are shown in Fig 7, for $n = 512$, $A = 0.95$, $L = 5$, $m = 3$. In addition, The sensitivity, specificity, and F1 score are listed in Table VI. The values of the specific indexes are obtained from the three coupled Lorenz oscillators with varying length of time series from 256 to 1024 and the remaining parameters are the same. The F1 scores of the proposed methods are much higher than the traditional PMIME method. The M-PMIME method performs best when the time series is short. That is to say, the mixed strategy plays a role in improving the F1 score. However, the F1 score of the LM-PMIME method is the highest as the length of the time series increases.

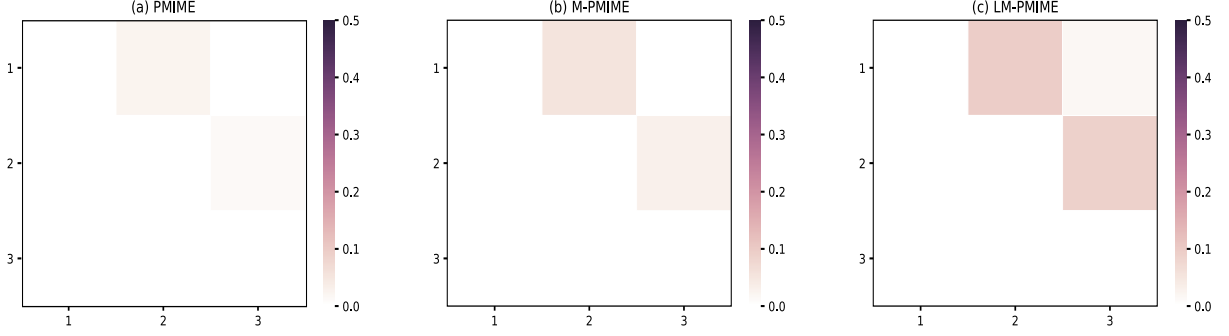


Figure 7 Matrix representation of causality for the three coupled Lorenz oscillators. Retrieved by traditional PMIME method (a), M-PMIME method (b), and LM-PMIME method (c) with k-NNs estimator. The length of the time series is 512 with coupling strength $C = 3$. $m = 3$ is used for the M-PMIME method and the LM-PMIME method. The remaining parameters of the three methods are the same ($L = 5$, $A = 0.95$). Color maps for the mean values of coupling measurements are obtained from 100 realizations of the three coupled Lorenz oscillators. The direction of causal influence is from row to column in the matrix. The true causal connections in the three coupled Lorenz oscillators are at the matrix elements $(i - 1, i)$, where $i = 2, 3$.

TABLE VI Sensitivity, specificity, and F1 score are obtained from 100 realizations of the three coupled Lorenz oscillators ($C = 3$) with varying length of time series for the three different methods. $A = 0.95$ and $L = 5$ are the parameters common to the three methods. In addition, the LM-PMIME method and the M-PMIME method use the parameter $m = 3$.

	Sensitivity	Specificity	F1 score
$n = 256$			
PMIME	0.225	0.997	0.364
M-PMIME	0.660	0.863	0.617
LM-PMIME	0.805	0.665	0.541
$n = 512$			
PMIME	0.185	1.000	0.312
M-PMIME	0.640	0.913	0.658
LM-PMIME	0.875	0.743	0.631
$n = 1024$			
PMIME	0.175	1.000	0.297
M-PMIME	0.670	0.909	0.674
LM-PMIME	0.970	0.756	0.687

The sensitivity, specificity, and F1 score are obtained from 100 realizations of the three coupled Lorenz oscillators with coupling strength C from 1 to 5 for the three different methods. The length of the time series is 512 and $A = 0.95$, $L = 5$, $m = 3$. The values of sensitivity, specificity, and F1 score are listed in Table VII. The results show that the LM-PMIME method performs best when the coupling strength C is low, such as $C = 1$. Although the F1 score of the traditional PMIME method increases as the coupling strength C increases, it is still much worse than the proposed methods. Fig 8 is the matrix representation of causality for the three coupled Lorenz oscillators with coupling strength $C = 5$. The true causal connections are $(i - 1, i)$ in the matrix elements, where $i = 2, 3$. Only for the LM-PMIME method, the mean values of coupling measurements on these matrix elements are positive and high.

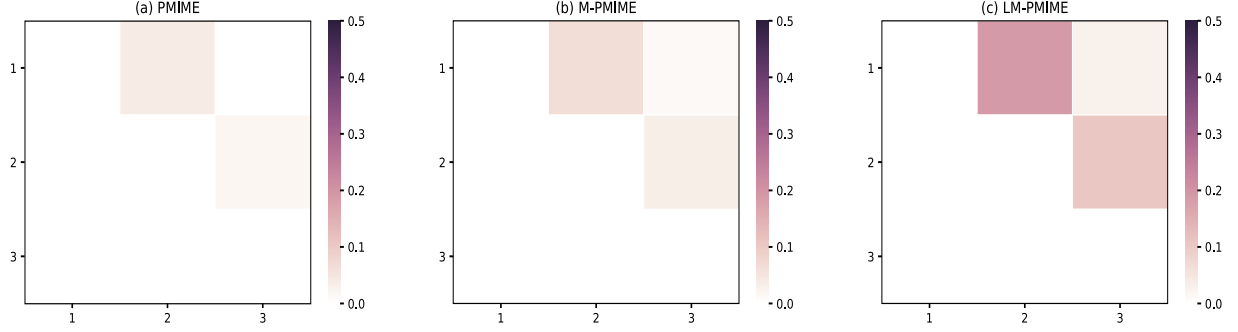


Figure 8 Matrix representation of causality for the three coupled Lorenz oscillators. Retrieved by traditional PMIME method (a), M-PMIME method (b), and LM-PMIME method (c) with k-NNs estimator. The length of the time series is 512 with coupling strength $C = 5$. $m = 3$ is used for the M-PMIME method and the LM-PMIME method. The remaining parameters of the three methods are the same ($L = 5$, $A = 0.95$). Color maps for the mean values of coupling measurements are obtained from 100 realizations of the three coupled Lorenz oscillators. The direction of causal influence is from row to column in the matrix. The true causal connections in the three coupled Lorenz oscillators are at the matrix elements $(i - 1, i)$, where $i = 2, 3$.

TABLE VII Sensitivity, specificity, and F1 score are obtained from 100 realizations of the three coupled Lorenz oscillators ($n = 512$) with coupling strength C from 1 to 5 for the three different methods. $A = 0.95$ and $L = 5$ are the parameters common to the three methods. In addition, the LM-PMIME method and the M-PMIME method use the parameter $m = 3$.

	Sensitivity	Specificity	F1 score
$C = 1$			
PMIME	0.000	1.000	0.000
M-PMIME	0.155	0.926	0.221
LM-PMIME	0.375	0.830	0.381
$C = 2$			
PMIME	0.075	1.000	0.141
M-PMIME	0.565	0.893	0.583
LM-PMIME	0.825	0.765	0.623
$C = 3$			
PMIME	0.185	1.000	0.312
M-PMIME	0.640	0.913	0.658
LM-PMIME	0.875	0.743	0.631
$C = 4$			
PMIME	0.260	1.000	0.413
M-PMIME	0.740	0.892	0.698
LM-PMIME	0.920	0.710	0.627
$C = 5$			
PMIME	0.320	0.997	0.481
M-PMIME	0.725	0.873	0.660
LM-PMIME	0.960	0.731	0.661

3.6. Coupled map lattice

The last simulated process is a ring lattice of K unidirectionally coupled tent maps [8, 32] defined as

$$\begin{cases} x_{i,t} = f[Cx_{i-1,t-1} + (1 - C)x_{i,t-1}], \\ i = 1, \dots, K (x_1 = x_K), \end{cases} \quad (15)$$

where $f(x) = 1 - 2|0.5 - x|$ and $K = 4$. The coupling strength is varied from $C = 0.01$ to $C = 0.05$ and the step is 0.01. The true causal connections in the process are $X_{i-1} \rightarrow X_i$ and $X_i \rightarrow X_1$, where

$i = 2, 3, 4$. The results are obtained from 100 realizations of the coupled map lattice for all methods. The length of the time series is 1024 and $A = 0.95$, $L = 5$, $m = 2$. The values of sensitivity, specificity, and F1 score are listed in Table VIII.

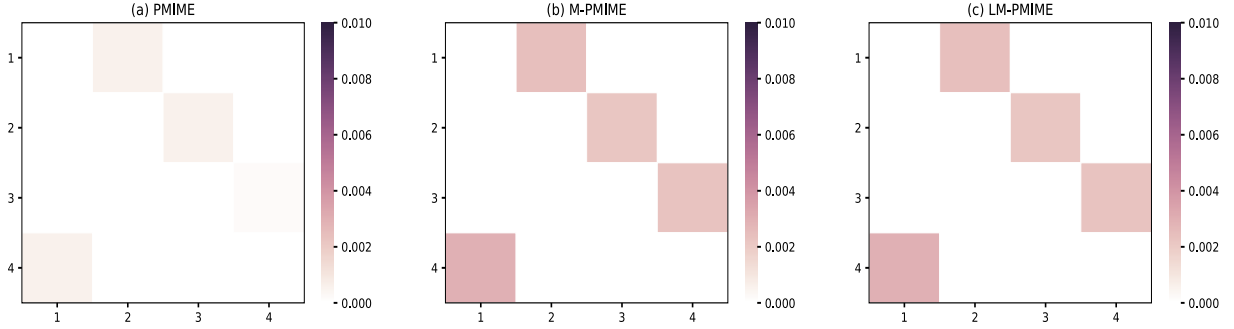


Figure 9 Matrix representation of causality for the coupled map lattice. Retrieved by traditional PMIME method (a), M-PMIME method (b), and LM-PMIME method (c) with k-NNs estimator. The length of the time series is 1024 with coupling strength $C = 0.04$. $m = 2$ is used for the M-PMIME method and the LM-PMIME method. The remaining parameters of the three methods are the same ($L = 5$, $A = 0.95$). Color maps for the mean values of coupling measurements are obtained from 100 realizations of the coupled map lattice. The direction of causal influence is from row to column in the matrix. The true causal connections in the process are at the matrix elements $(i - 1, i)$ and $(i, 1)$, where $i = 2, 3, 4$.

TABLE VIII Sensitivity, specificity, and F1 score are obtained from 100 realizations of coupled map lattice ($n = 1024$) with coupling strength C from 0.01 to 0.05 for the three different methods. $A = 0.95$ and $L = 5$ are the parameters common to the three methods. In addition, the LM-PMIME method and the M-PMIME method use the parameter $m = 2$.

	Sensitivity	Specificity	F1 score
$C = 0.01$			
PMIME	0.000	1.000	0.000
M-PMIME	0.000	1.000	0.000
LM-PMIME	0.010	0.989	0.019
$C = 0.02$			
PMIME	0.000	1.000	0.000
M-PMIME	0.000	1.000	0.000
LM-PMIME	0.035	0.986	0.065
$C = 0.03$			
PMIME	0.000	1.000	0.000
M-PMIME	0.003	1.000	0.005
LM-PMIME	0.030	0.994	0.058
$C = 0.04$			
PMIME	0.055	1.000	0.104
M-PMIME	0.443	1.000	0.614
LM-PMIME	0.198	0.998	0.328
$C = 0.05$			
PMIME	0.697	0.991	0.809
M-PMIME	1.000	1.000	1.000
LM-PMIME	0.835	1.000	0.910

When the coupling strength $C = 0.01$, the F1 scores of the PMIME method and the M-PMIME method are 0. But the F1 score of the LM-PMIME method is slightly better than the others. That

is to say, the low-dimensional approximation of CMI can improve the effect of causal analysis when the coupling strength is weak. In addition, the results of the proposed methods are better than the traditional PMIME method with the increase of coupling strength. Fig 9 is the matrix representation of causality for the coupled map lattice with coupling strength $C=0.04$. The true causal connections are $(i-1, i)$ and $(i, 1)$ in the matrix elements, where $i = 2, 3, 4$. The coupling measured by the proposed methods are generally high. In contrast, the traditional PMIME method measures lower values, especially in matrix element $(3, 4)$.

4. Application

In this section we show the applicability of the proposed LM-PMIME method to actual electrocorticographic (ECoG) data. That is to say, through the causal analysis method to explore key contacts of the human subject with intractable epilepsy and assist doctors in the diagnosis and treatment of the disease. A public dataset from the human subject (a 39-year-old woman with medically refractory complex partial seizures) is used. The dataset contains 8 seizure epochs and 8 pre-seizure epochs. Each epoch contains 76 time series obtained from the 8-by-8 electrode grid and two depth electrodes with six contacts each. In addition, the duration of each epoch is 10s and the length of each time series is 4000 (More details about the data are given in [33]).

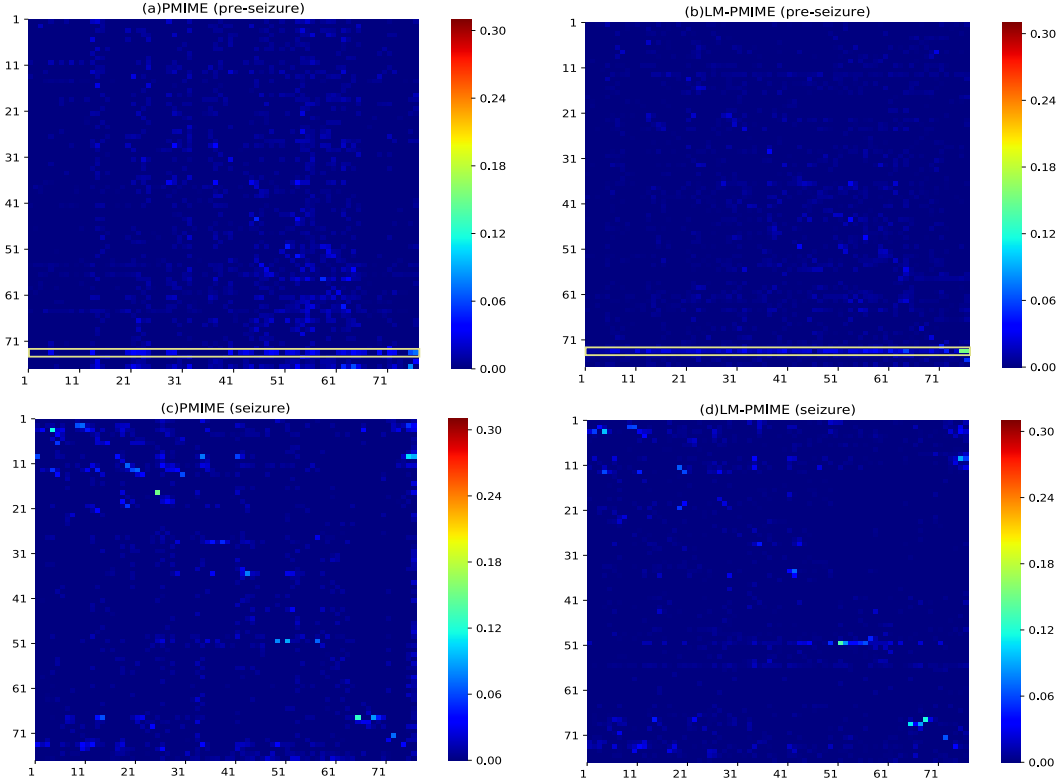


Figure 10 Results for multivariate electrocorticographic (ECoG) data. Matrices of causalities reflect the pre-seizure state (top) and the seizure state (down) estimated by the PMIME method and the LM-PMIME method. The causal strengths are averaged (the mean values of the coupling measurements over all epochs in the same physiological state). Contacts 1 to 64 belong to an 8-by-8 electrode grid, and contacts 65 to 76 belong to two depth electrodes. The direction of causal influence is from row to column in the matrices. The brighter colors indicate more significant values. The key contact is marked by a rectangular box. The parameter $A = 0.95$ and $m = 2$ are set for the different methods.

We use PMIME method and LM-PMIME method to analyze the seizure data and the pre-seizure data. The data were recorded at a fixed sampling rate of 400 Hz which were downsampled to 100 Hz. To assess the causal matrices of different physiological states estimated by each method, we compute the average causal strengths (the mean values of the coupling measurements over all epochs in the same physiological state) as shown in Fig. 10. The brighter the colors are, the more significant causal connections exist. As a result, it is obvious from the causal matrices of LM-PMIME method that contact 73 has more impact to the other contacts, highlighting that it is the key contact in the pre-seizure data [see Fig. 10(b)]. However, the traditional PMIME method has led to a lot of false positives [see Fig. 10(a)]. Fig. 11 illustrates the difference of total numbers of significant connections between the seizure state and the pre-seizure state. The proposed method highlights the key contact 50 [see Fig. 11(b)] and these discovered key contacts are consistent with many researchers [33–35].

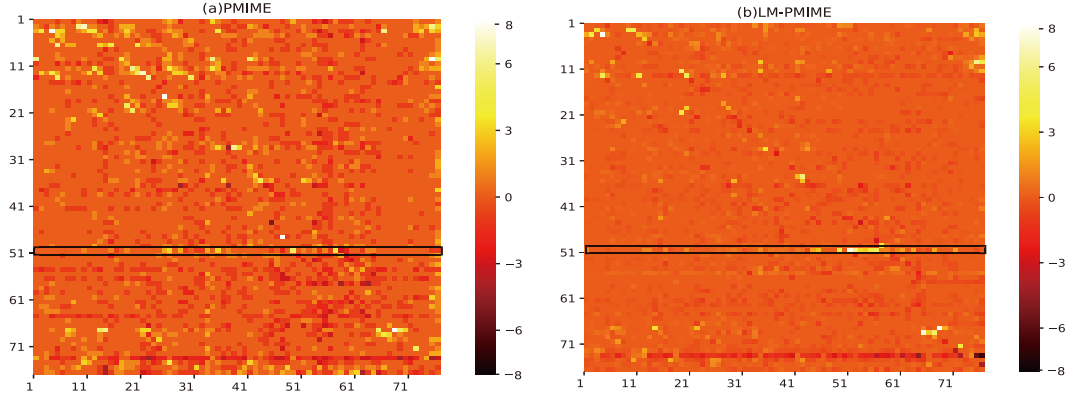


Figure 11 Results for multivariate electrocorticographic (ECoG) data. Matrices reflect the difference of total numbers of significant connections between the seizure state and the pre-seizure state (seizure minus pre-seizure). The numbers are respectively summed from 8 seizure epochs and 8 pre-seizure epochs. Contacts 1 to 64 belong to an 8-by-8 electrode grid, and contacts 65 to 76 belong to two depth electrodes. The direction of causal influence is from row to column in the matrices. The brighter colors indicate more significant values. The key contact is marked by a rectangular box. The parameter $A = 0.95$ and $m = 2$ are set for the different methods.

We observe that LM-PMIME method gives an obvious causal driver located at the contact 73 from the second depth electrode strip in the pre-seizure data. Therefore, the contact 73 may be associated with seizures. Although not yet clinically observable, it has been suggested that the second depth electrode primarily affect cortical activity in [34, 35]. In addition, the proposed method successfully identifies a key contact from the data: contact 50, which exhibits the most significant change in the betweenness centrality. The contact is considered as the primary target of therapeutic intervention in [38], because contacts with statistically significant increases in betweenness centrality may lead to seizures. In contrast, traditional PMIME method leads to a large number of false positives so key contacts cannot be highlighted.

5. Discussion and conclusion

In this paper, we have put forward a new non-uniform embedding method named LM-PMIME for multivariate time series. We present effective modifications for the well-known non-uniform embedding method: PMIME, which quantifies causality by means of information theoretic measures. The advantage of the non-uniform embedding compared to uniform embedding is that it can reduce the dimension of the state space by selecting the relevant variables which contribute the most to explain the target

variable. Therefore it has been proved that the non-uniform embedding process is more flexible for state space reconstruction [8,9,36]. However, there are still some obstacles to estimate high-dimensional CMI and form optimal mixed embedding vector in the traditional non-uniform embedding methods. The proposed LM-PMIME method overcomes the shortcomings of traditional methods. The effectiveness and applicability of the LM-PMIME method are proved by a large number of experiments. Furthermore, the LM-PMIME method works well for multivariate time series with weak coupling strengths, especially for chaotic systems. The usefulness of the LM-PMIME method for multivariate time series is illustrated by the analysis of actual ECoG data.

The major contribution of the proposed LM-PMIME method is to improve the traditional methods based on the low-dimensional approximation of conditional mutual information and the mixed search strategy. The curse of dimensionality is avoided by replacing the original estimate with a low-dimensional approximation of conditional mutual information. In addition, a mixed strategy instead of the greedy strategy was used as an embedded strategy to solve the problem of initial embedding inaccuracy. Hence, the mixed embedding vector becomes more parsimonious by maximizing the correlation with the target variable and minimizing the redundancy between the selected variables. In order to solve these problems, there are also other propositions, for example, in [16] a preselection scheme for subsets of causal predictors is used to search an optimal subset and detect the synergetic variables. Different from these preselection schemes, the LM-PMIME method relies on both the low-dimensional approximation and the mixed search strategy to alleviate the conditions. In all simulation systems, the LM-PMIME method performs better than the traditional methods according to the F1 score. Because of the complexity of chaotic systems, true causal connections are often difficult to detect. However, the LM-PMIME method significantly improves the sensitivity in chaotic systems. In the remaining simulation systems, the LM-PMIME method reduces false positives and increases the specificity. The experiments also add a comparison method M-PMIME, which improve the search strategy without using low-dimensional approximation. Through the M-PMIME method, it can be found that the mixed search strategy works well in chaotic systems, especially the systems with low coupling strengths. The low-dimensional approximation of conditional mutual information plays an important role in linear and nonlinear systems. Therefore, we combine both the low-dimensional approximation of conditional mutual information and the mixed search strategy to form a new non-uniform embedding method LM-PMIME for multivariate time series.

Although the LM-PMIME method works better than the traditional method, there are limitations to the proposed method. It still does not exceed the efficiency of the standard uniform embedding methods under the non-uniform embedding framework [37]. In addition, the strategy adjustment factor m is larger, the traversal strategy is used more times in iterations. The main role of the traversal strategy is to correct the initial embedding inaccuracy, which is often time consuming. Therefore, the recommended value of m is less than 5 and the simulation results generally take $m = 2$ or $m = 3$ to achieve better results. Because a smaller value of m can reduce the computation time and it is enough to optimize the initial embedding. In this study, we focus on the causal analysis and the proposed LM-PMIME method can also be employed for other applications, e.g. prediction of dynamic systems and correlation analysis. We will further study the embedded approach and extend applications.

Acknowledgement

Financial supports by National Natural Science Foundation of China (61603029), and the Fundamental Research Funds for the Central Universities (2018RC002) are gratefully acknowledge.

References

- [1] Granger C W J. Investigating causal relations by econometric models and cross-spectral methods[J]. *Econometrica: Journal of the Econometric Society*, 1969: 424-438.
- [2] Marko H. The bidirectional communication theory—a generalization of information theory[J]. *IEEE Transactions on communications*, 1973, 21(12): 1345-1351.
- [3] Schreiber T. Measuring information transfer[J]. *Physical Review Letters*, 2000, 85(2): 461.
- [4] Barnett L, Barrett A B, Seth A K. Granger causality and transfer entropy are equivalent for Gaussian variables[J]. *Physical Review Letters*, 2009, 103(23): 238701.
- [5] Schindlerova K. Equivalence of Granger Causality and Transfer Entropy: A Generalization[J]. *Applied Mathematical Sciences*, 2011, 5: 36373648.
- [6] Mao X, Shang P. Transfer entropy between multivariate time series[J]. *Communications in Nonlinear Science and Numerical Simulation*, 2017, 47: 338-347.
- [7] Montalto A, Stramaglia S, Faes L, et al. Neural networks with non-uniform embedding and explicit validation phase to assess Granger causality[J]. *Neural Networks*, 2015, 71: 159-171.
- [8] Faes L, Nollo G, Porta A. Information-based detection of nonlinear Granger causality in multivariate processes via a nonuniform embedding technique[J]. *Physical Review E*, 2011, 83(5): 051112.
- [9] Vlachos I, Kugiumtzis D. Nonuniform state-space reconstruction and coupling detection[J]. *Physical Review E*, 2010, 82(1): 016207.
- [10] Kugiumtzis D. Direct-coupling information measure from nonuniform embedding[J]. *Physical Review E*, 2013, 87(6): 062918.
- [11] Kugiumtzis D, Koutlis C, Tsimpiris A, et al. Dynamics of epileptiform discharges induced by transcranial magnetic stimulation in genetic generalized epilepsy[J]. *International Journal of Neural Systems*, 2017, 27(07): 1750037.
- [12] Kugiumtzis D, Kimiskidis V K. Direct causal networks for the study of transcranial magnetic stimulation effects on focal epileptiform discharges[J]. *International Journal of Neural Systems*, 2015, 25(05): 1550006.
- [13] Papana A, Kyrtsov C, Kugiumtzis D, et al. Financial networks based on Granger causality: A case study[J]. *Physica A: Statistical Mechanics and its Applications*, 2017, 482: 65-73.
- [14] Papana A, Kyrtsov C, Kugiumtzis D, et al. Assessment of resampling methods for causality testing: A note on the US inflation behavior[J]. *PloS one*, 2017, 12(7): e0180852.
- [15] Runge J, Heitzig J, Petoukhov V, et al. Escaping the curse of dimensionality in estimating multivariate transfer entropy[J]. *Physical Review Letters*, 2012, 108(25): 258701.
- [16] Runge J, Donner R V, Kurths J. Optimal model-free prediction from multivariate time series[J]. *Physical Review E*, 2015, 91(5): 052909.
- [17] Brown G, Pocock A, Zhao M J, et al. Conditional likelihood maximisation: a unifying framework for information theoretic feature selection[J]. *Journal of Machine Learning Research*, 2012, 13: 27-66.

- [18] Vinh N X, Zhou S, Chan J, et al. Can high-order dependencies improve mutual information based feature selection?[J]. *Pattern Recognition*, 2016, 53: 46-58.
- [19] Wibral M, Vicente R, Lizier JT. *Directed Information Measures in Neuroscience*. Berlin; Heidelberg: Springer-Verlag. 2014.
- [20] Battiti R. Using mutual information for selecting features in supervised neural net learning[J]. *IEEE Transactions on Neural Networks*, 1994, 5(4): 537-550.
- [21] Yang H H, Moody J. Data visualization and feature selection: New algorithms for nongaussian data[C]. *Advances in Neural Information Processing Systems*. 2000: 687-693.
- [22] Fleuret F. Fast binary feature selection with conditional mutual information[J]. *Journal of Machine Learning Research*, 2004, 5 : 1531-1555.
- [23] Peng H, Long F, Ding C. Feature selection based on mutual information criteria of max-dependency, max-relevance, and min-redundancy[J]. *IEEE Transactions on Pattern Analysis and Machine Intelligence*, 2005, 27(8): 1226-1238.
- [24] Lin D, Tang X. Conditional infomax learning: an integrated framework for feature extraction and fusion[C]. *European Conference on Computer Vision*. Springer, Berlin, Heidelberg, 2006: 68-82.
- [25] Meyer P E, Bontempi G. On the use of variable complementarity for feature selection in cancer classification[C]. *Workshops on Applications of Evolutionary Computation*. Springer, Berlin, Heidelberg, 2006: 91-102.
- [26] Hacine-Gharbi A, Ravier P, Harba R, et al. Low bias histogram-based estimation of mutual information for feature selection[J]. *Pattern Recognition Letters*, 2012, 33(10): 1302-1308.
- [27] Kwak, N, Choi, C. H. Input feature selection by mutual information based on Parzen window. *IEEE Transactions on Pattern Analysis and Machine Intelligence*, 2002 (12): 1667-1671.
- [28] Kraskov A, Stgbauer H, Grassberger P. Estimating mutual information[J]. *Physical Review E*, 2004, 69(6): 066138.
- [29] Schelter B, Winterhalder M, Hellwig B, et al. Direct or indirect? Graphical models for neural oscillators[J]. *Journal of Physiology-Paris*, 2006, 99(1): 37-46.
- [30] Zhang J. Low-dimensional approximation searching strategy for transfer entropy from non-uniform embedding[J]. *PloS one*, 2018, 13(3): e0194382.
- [31] Gourvitch B, Le Bouquin-Jeanns R, Faucon G. Linear and nonlinear causality between signals: methods, examples and neurophysiological applications[J]. *Biological cybernetics*, 2006, 95(4): 349-369.
- [32] Romano M C, Thiel M, Kurths J, et al. Estimation of the direction of the coupling by conditional probabilities of recurrence[J]. *Physical Review E*, 2007, 76(3): 036211.
- [33] Kramer M A, Kolaczyk E D, Kirsch H E. Emergent network topology at seizure onset in humans[J]. *Epilepsy Research*, 2008, 79(2-3): 173-186.
- [34] Marinazzo D, Pellicoro M, Stramaglia S. Kernel method for nonlinear Granger causality[J]. *Physical Review Letters*, 2008, 100(14): 144103.

- [35] Faes L, Marinazzo D, Stramaglia S. Multiscale information decomposition: exact computation for multivariate Gaussian processes[J]. Entropy, 2017, 19(8): 408.
- [36] Porta A, Faes L. WienerGranger causality in network physiology with applications to cardiovascular control and neuroscience[J]. Proceedings of the IEEE, 2016, 104(2): 282-309.
- [37] Montalto A, Faes L, Marinazzo D. MuTE: a MATLAB toolbox to compare established and novel estimators of the multivariate transfer entropy[J]. PloS one, 2014, 9(10): e109462.